Memoirs of the School of Engineering, Nagoya University
Vol.50, No.1 (1998)

SHAPE OPTIMIZATION OF SHELL AND SPATIAL STRUCTURE FOR SPECIFIED STRESS DISTRIBUTION

Hiroshi OHMORI* and Kenji YAMAMOTO†

Department of Architecture

(Received December 4, 1997)

Abstract

Shells and spatial structures are adopted for construction of large span structures in which a large space is realized without columns as the structural components. In those cases, the structures are expected to resist against various design loads mainly through their extremely strong capability which can be acquired through in-plane or membrane stress resultants and this is just the reason by which they themselves stand for external loads without columns as their structural components in the large span structures.

Up to this time, shells and spatial structures have been frequently adopted as a structure which can realize large span constructions, where, however, purely geometrical shapes like spheres, cylinders and their parts have been adopted as their structural forms. It can be said relatively easy to handle purely geometrical shapes from the view-point of both structural analysis and construction design, where, however, we have to handle bending stress resultants which are inevitably accompanied with especially in the vicinity of their supporting boundaries. From the view point as mentioned above about the mechanical characteristics of shell and spatial structure, it would be consistent if we could have those bending stresses rationally treated not through cheap tricks like addition of shell thickness but some essential treatments which are originated from the investigation of the forms themselves of the structures.

In the present work, direct treatment method of stress distribution in shells and spatial structures are shown, which enables us to obtain approximately bending free structural forms. Numerical calculation has been carried out for both axisymmetric shells and spatial structures, where effectiveness of this method has been clearly shown and mechanical characteristics of the obtained surface of both shells and spa-

*Department of Architecture, School of Engineering, Nagoya University
†Department of Architecture, Faculty of Engineering, Kagoshima University

tial structures are discussed as well. Finally, some feasibility studies adopting RC shells as an example are also shown.

Keywords: shape optimization, sensitivity analysis, shell, space structure, space frame, bending moment, nonlinear programing, sequential programing method

Contents

1 Introduction

Shells and spatial structures are adopted for construction of large span structures in which a large space is realized without columns as the structural components. In those cases, the structures are expected to resist against various design loads mainly through their extremely strong capability which can be acquired through in-plane or membrane stress resultants and this is just the reason by which they themselves stand for external loads without columns as their structural components in the large span structures. It is the reason why some researchers call the mechanical system of such structures “shape resistant structure”[1)]. Up to this time, shells and spatial structures have been frequently adopted as a structure which can realize large span constructions, where, however, purely geometrical shapes like spheres, cylinders and their parts have been adopted as their structural forms[2)]. It can be said relatively easy to handle purely geometrical shapes from the view-point of

both structural analysis and construction design, where, however, we have to handle bending stress resultants which are inevitably accompanied with especially in the vicinity of their supporting boundaries. From the view point as mentioned above about the mechanical characteristics of shell and spatial structure, it would be consistent if we could have those bending stresses rationally treated not through cheap tricks like addition of shell thickness but some essential treatments which are originated from the investigation of the forms themselves of the structures[3,1)]. The previous work[4)] has shown how to obtain the hanging forms which enables us to directly get bending-free structural forms under dead load due to arbitrary boundary conditions for shells and spatial structures, where variational principle has been applied to the hanging membrane with some subsidiary conditions as restraints with respect to the total surface area of the objective surface. In the present work, direct treatment method of stress distribution in shells and spatial structures are shown, which enables us to obtain approximately bending free structural forms. Numerical calculation has been carried out for both axisymmetric shells and spatial structures, where effectiveness of this method has been clearly shown and mechanical characteristics of the obtained surface of both shells and spatial structures are discussed as well. Finally, some feasibility studies adopting RC shells as an example are also shown.

2 Theory

2.1 Objective Function

The objective function of the present problem can be shown by utilizing the least square method as follows;

$$J = \sum_e \int_S M_i^2 \, ds \quad (i = 1, 2, 3) \quad \rightarrow \quad Min. \tag{1}$$

where M_i represents the component of the bending moment in the i-th direction and finite element method is assumed to be used. The integral should be taken through one element and the summation for all elements of the surface. Minimization has to be carried out with respect to position vector $\boldsymbol{r}$ of nodes of finite elements. Furthermore, bending moment components in Eq. 1 are functions of nodal displacements $\boldsymbol{d}$. Consequently, the objective function J of the present problem can be expressed as follows;

$$J = J(\boldsymbol{r}, \boldsymbol{d}(\boldsymbol{r})) \tag{2}$$

2.2 Finite Element Formulation for Axisymmetric Shells

Finite element for axisymmetric shell used in the present paper is the ordinary one as shown in Fig. 1, where, as in the usual treatment, the first order algebraic functions are adopted for expression of the in-plane displacements and, on the other hand, the third order one is used for that of the out-plane displacement. In the present analysis, only symmetric components of displacements with respect to $\theta = 0$ are considered and homogeneously isotropic materials are assumed for the shell. Consequently, the objective function can be expressed as follows;

$$J = \sum_e \sum_n \boldsymbol{d}_n^T \Gamma_n \, \boldsymbol{d}_n \tag{3}$$

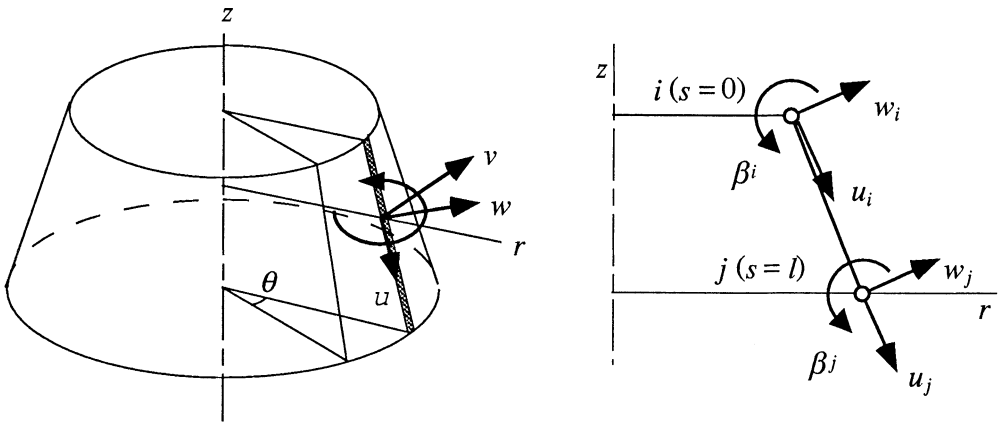

Fig. 1: Axisymmetric Finite Element (Conical Element)

where

$$\Gamma_n = \pi \ell \int_0^1 \boldsymbol{B}_n^T \boldsymbol{D}^T \boldsymbol{D} \boldsymbol{B}_n r(\xi)\, d\xi \tag{4}$$

and, $\boldsymbol{B}_n$ and $\boldsymbol{D}$ represent the strain-displacement matrix and the elastic matrix, respectively. As, we can see from the expression of Eq. 3, the present problem has been reduced to the minimization problem of objective function J with respect to the position vector $\boldsymbol{r}$ which expresses the nodal coordinates of shell elements.

2.3 Finite Element Formulation for Spatial Structures

Finite element for spatial structures used in the present paper is the ordinary three dimensional beam element as shown in Fig. 2, where, as in the previous section for the axisymmetric shell element, the first order algebraic functions are adopted for expression of the in-plane displacements and, on the other hand, the third order one is used for that of the out-plane displacement. Assuming homogeneously isotropic materials, the objective function of the present problem can be obtained as follows;

$$J = \sum_e \boldsymbol{d}^T \Gamma \boldsymbol{d} \tag{5}$$

where

$$\Gamma = \ell \int_0^1 \boldsymbol{B}^T \boldsymbol{D}^T \boldsymbol{D} \boldsymbol{B}\, d\xi \tag{6}$$

and, $\boldsymbol{B}$ and $\boldsymbol{D}$ represent the strain-displacement matrix and the elastic matrix, respectively. Consequently, as in the same manner in the previous section for the axisymmetric shells, the minimiza-

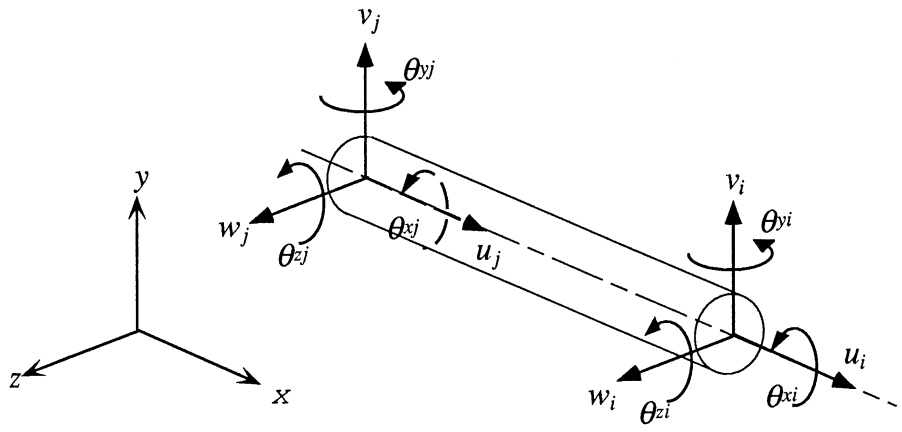

Fig. 2: Beam Finite Element

tion problem with respect to position vector $\boldsymbol{r}$ of the nodes of finite elements has been obtained.

2.4 Introduction of Constraint Conditions

It has been experienced through our previous researches[5,6,7] that introduction of some constraint conditions into the nonlinear programming problem efficie tly works because it can make narrow the searching space of the problem. For the present problem, following restraint conditions are introduced for each problem, respectively.

$$J = \sum_e \int_S M_i^2 ds \quad \rightarrow \quad Min. \tag{7}$$
$$Subject\ to\ S = S_0$$

$$J = \sum_e \int_L M_i^2 dL \quad \rightarrow \quad Min. \tag{8}$$
$$Subject\ to\ L = L_0$$

Eq. 7 is set for axisymmetric shells and Eq. 8 for spatial structures, where S_0 and L_0 represent specified values for total surface area of the shell and total length of the structural element of the spatial structure, respectively.

3 Numerical Analysis of Shape Optimization of Shells

Numerical examples of shape optimization for axisymmetric shells are presented in this section, where dome shells subjected to both snow and wind loads, respectively, besides dead load are dealt with as design loads.

3.1 Dome under Dead Load

Table 1: Parameters adopted for Dome Analysis subjected to Dead Load

Number of Node	41	Young's Modulus	2.1×10^6 tf/m^2
Number of Element	40	Poisson's Ratio	0.17
Degree of Freedome	40 (z-free)	Weight Density	2.4 t/m^3
Span	30 m	Shell Thickness	0.1 m

As the first numerical example for shape optimization of shells, results for a dome shell subjected to its dead load are shown in this section. Fundamental data used in numerical analysis are as shown in Table 1. As the initial shape, a spherical shell is adopted, of which diameter is 30 m and surface area 800 m^2, where the initial value of surface area of the sphere is used as the restraint condition for nonlinear programming problem. As boundary conditions, three types are considered, that is, an inclined roller, a fixed and a pinned supporting condition, respectively.

Figs. 3a through 3d show the results for the inclined roller supporting condition, Figs. 4a through 4d for the fixed one and Figs. 5a through 5d for the pinned supporting condition, where the restraint conditions of the surface area given from the initial spherical shell are imposed. In each figure of Figs. 3a through 5d, Figs. a, b, c and d show the shape of shell section along the longitudinal line, the membrane stress distribution, the bending stress distribution and the displacement in the out-plane direction in the vicinity of the boundary, respectively, comparing the results of the initial shape with those of the finally obtained shape. Occurrence of the bending stress is clearly shown to be suppressed in the case of the dome with the inclined roller supporting condition. Comparison of the displacement modes between those of the initial shape and of the finally obtained shape tells us the mechanism of reduction of the bending moment in the vicinity of the boundary, where we can find final shape for each case of boundary condition. On the other hand, it can be observed that the bending moment stresses initially occurred in the vicinity of the boundaries are averagely suppressed and, although the amount is not so large, there can be seen the presence of the bending stresses in some parts where no bending stress existed initially, as if the excess amount of the bending stress were re-distributed. This should be explained as the result of the usage of the least square method as an minimization technique.

3.2 Dome under Several Design Loads

3.2.1 Snow Load

In present section, the results of shape analysis of axisymmetric shell subjected to snow load besides self weight are shown. The snow load is assumed to be as shown in Fig. 6, where two loading cases are considered, that is, homogeneously full loading (Case A) and eccentrically partial one (Case B), respectively. The fundamental data used in numerical analysis are as shown in Table 2. The initial data for the nonlinear analysis are taken from those of the spherical shell as same as those of the previous section. Fixed boundary condition is adopted. Numerical results for the present analysis are shown in Figs. 7 through 9, where Figs. a, b and c show the shape of the shell section along longitudinal line, the stress distribution for the loading case A and that for the case B, respectively. Because there is not so big difference between the load of dead and snow loading fully acted, Fig. 8 shows the similar results as those shown in Fig. 4b through Fig. 4c. On the other hand, a relatively large change in bending moment can be seen in Fig. 9 for partial load-

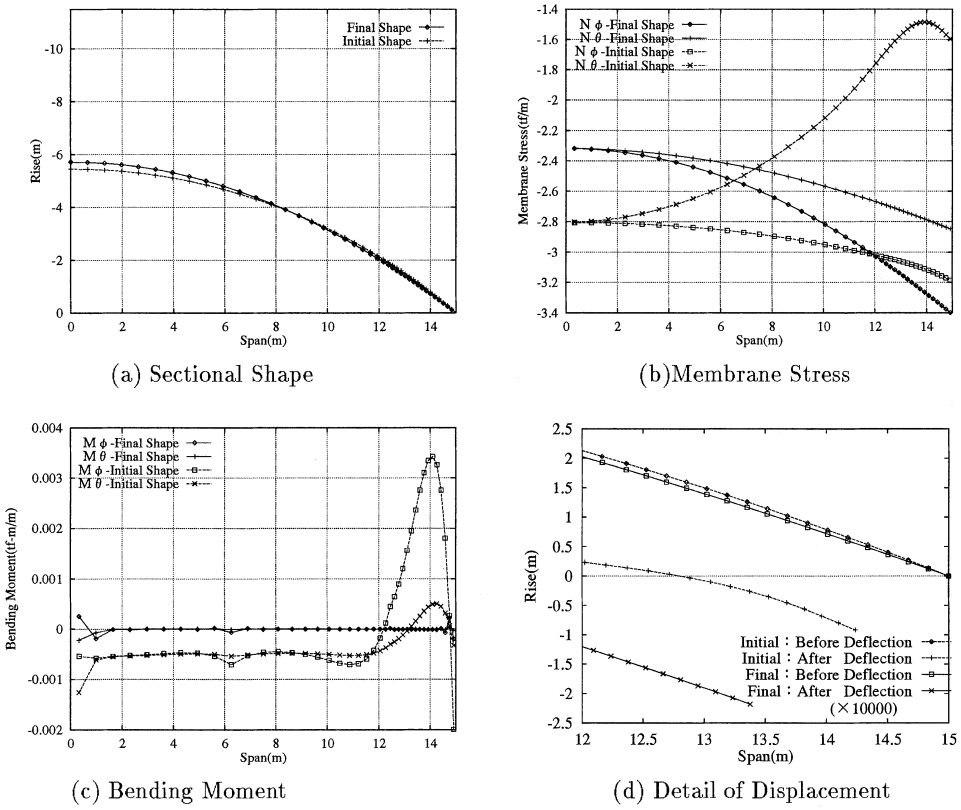

Fig. 3: Results of Shape Analysis (Dead Load, Inclined Roller Support)

ing case and, nevertheless, the bending stress distribution seen in the vicinity around the edge of the loading area in the shell of the initial shape can be understood to be suppressed up to a certain amount in the final shape.

3.2.2 Wind Load

This section represents the numerical results where wind loadings are subjected to axisymmetric shells besides dead load as the external loadings. Fundamental data used for numerical analysis are as shown in Table 3 and the initial shape is taken from the spherical shell as up to the previous analyses, that is, 30 m for diameter and 800 m^2 for constraint value of surface area of the shell. Wind load adopted in the present analysis is as described as follows;

$$w = c\,q \tag{9}$$

where

$$c = -1.4 + (0.9 + 0.6\cos\theta + 0.9\cos 2\theta)\cos\varphi \tag{10}$$

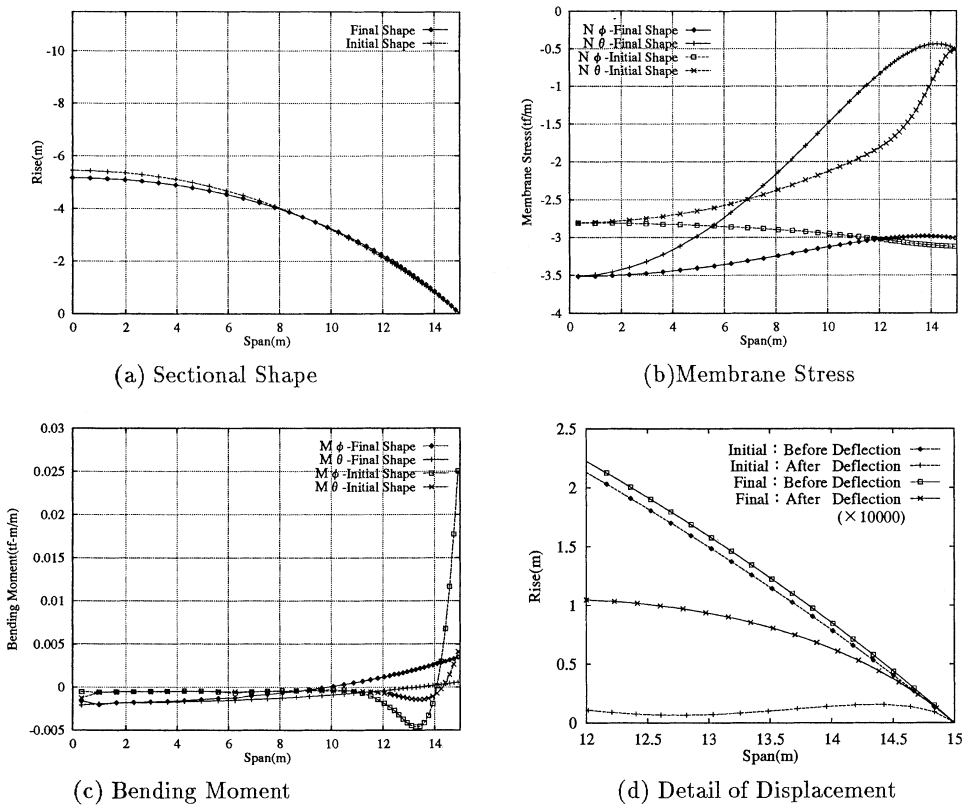

Fig. 4: Results of Shape Analysis (Dead Load, Fixed Support)

and, w, q and c represent a wind pressure, a wind velocity and a coefficient of wind load, respectively. Fig. 10 shows spatial distribution of the wind load. Numerical results of the present analysis are shown in Figs. 11 through 14, where each figure shows the shape of the shell section along the longitudinal line, the bending moment in the longitudinal direction, the bending moment in the meridional direction and the twisting moment, respectively, together with comparison of those results between initial and final shapes. At this point, we have to pay attention to the fact that the present analysis is performed by taking only 0-th order of Fourier expansion in the circumstance direction for expression of the shell shape itself while the response analysis is carried out by taking up to the specified number of Fourier expansion in the circumstance direction as well as 0-th order of Fourier expansion component. As it can be seen from the expression of Eq. 9, external loads are subjected to the shell being expanded in such manner that it includes anti-axisymmetric components having wave numbers in the circumstance direction more than 0 as well as axisymmetric one. As a result, although it is natural that various responses, that is, stresses and displacements respond anti-axisymmetrically, the shape search itself is nevertheless done within the limited space where only axisymmetric change is allowed. In another word, it can be said that the present shape analysis of the asymmetric shell is carried out under the restraint condition by which only 0-th order component is allowed to occur and the occurrence of the other components are suppressed in expression of the shape of the shell. Taking into account that the direction to the shell of the wind

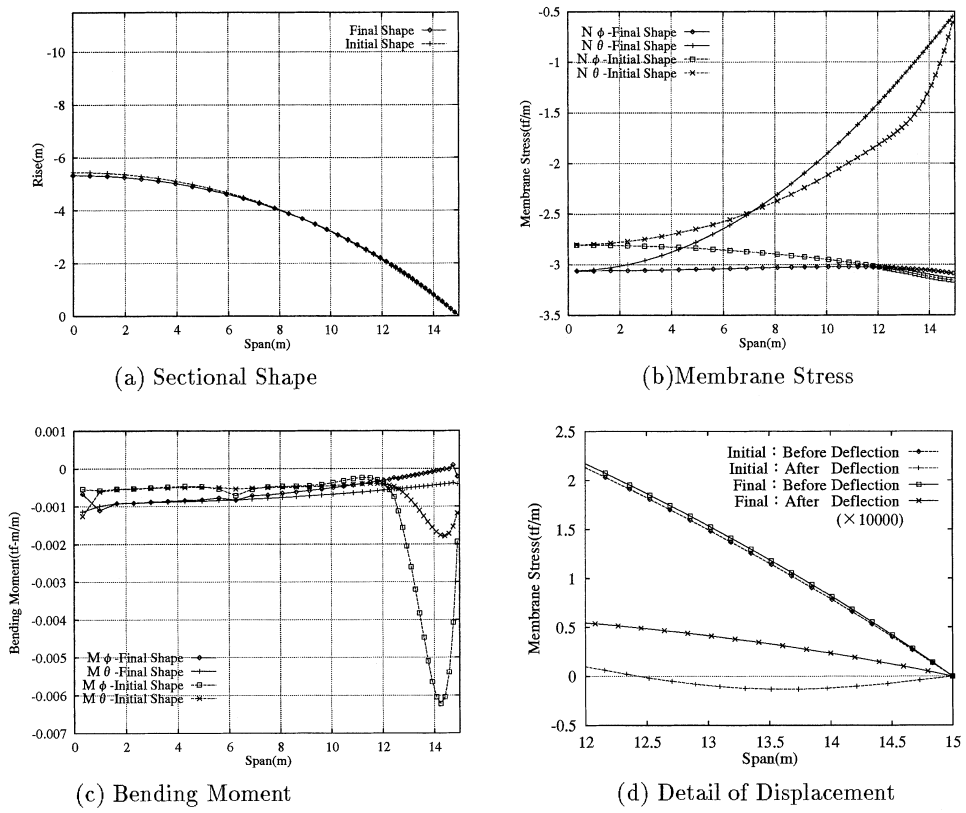

Fig. 5: Results of Shape Analysis (Dead Load, Pinned Support)

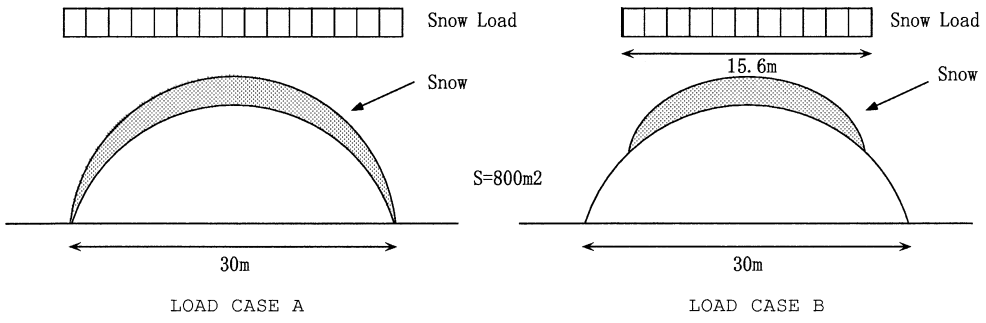

Fig. 6: Snow Load

load is indefinite, it is rather natural to assume the change of the shell to be in such a way that expression of the shape of the shell includes only 0-th order of Fourier expansion component. Figs. 11 through 14b show the numerical results where the wind load including the anti-axisymmetric components is subjected to the axisymmetric shell besides the dead load. It can be clearly said

Table 2: Parameters adopted for Dome Analysis subjected to Snow Load

Number of Node	41	Young's Modulus	2.1×10^6 tf/m^2
Number of Element	40	Poisson's Ratio	0.17
Degree of Freedome	40 (z-free)	Weight Density	2.4 t/m^3
Span	30 m	Snow Load	40 kg/m^2
Shell Thickness	0.1 m		

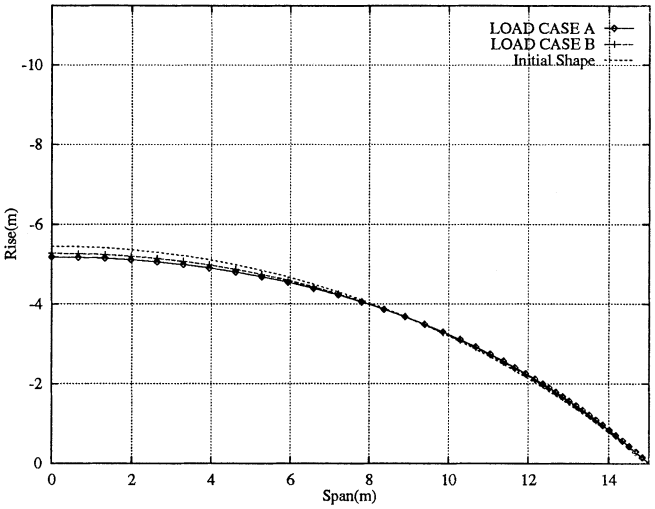

Fig. 7: Sectional Shape along the Longitudinal Line (Snw Load + Dead Load, Fixed Support)

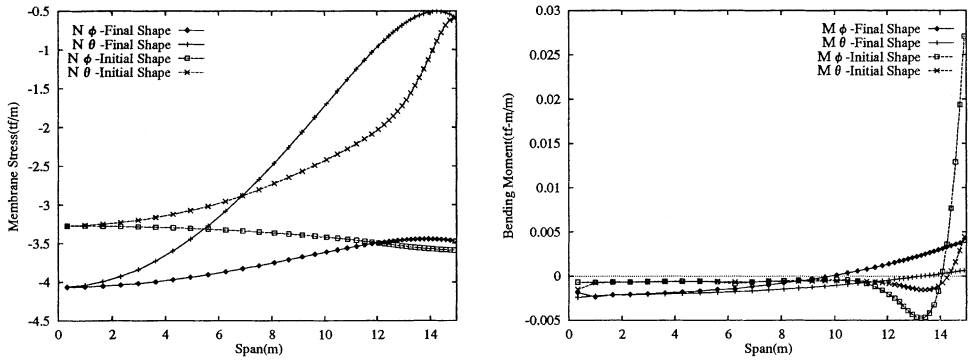

Fig. 8: Stress Distributions for Loading Case A

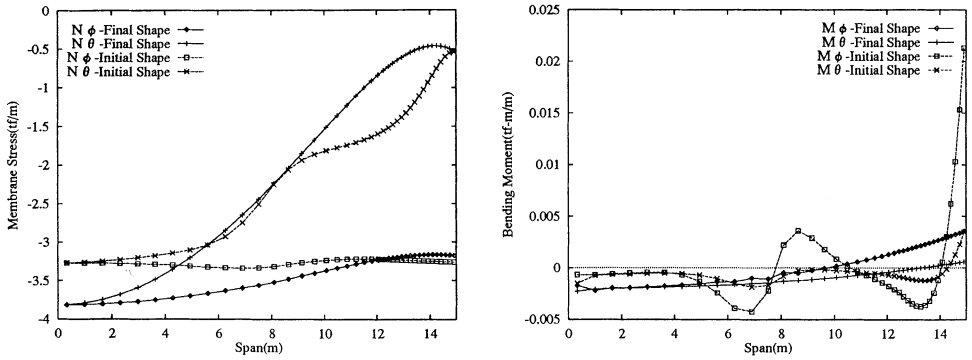

Fig. 9: Stress Distributions for Loading Case B

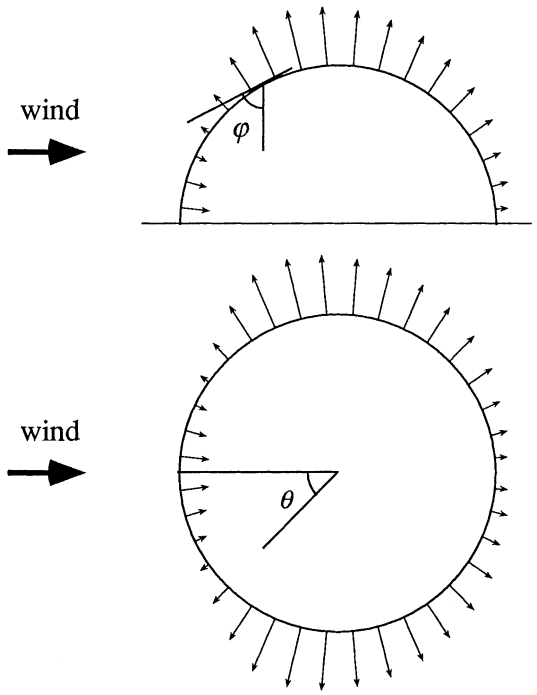

Fig. 10: Wind Load

Table 3: Parameters adopted for Dome Analysis subjected to Wind Load

Number of Node	41	Young's Modulus	2.1×10^6 tf/m^2
Number of Element	40	Poisson's Ratio	0.17
Degree of Freedome	40 (z-free)	Weight Density	2.4 t/m^3
Span	30 m	Velocity Pressure	56.3 kg/m^2
Shell Thickness	0.1 m		

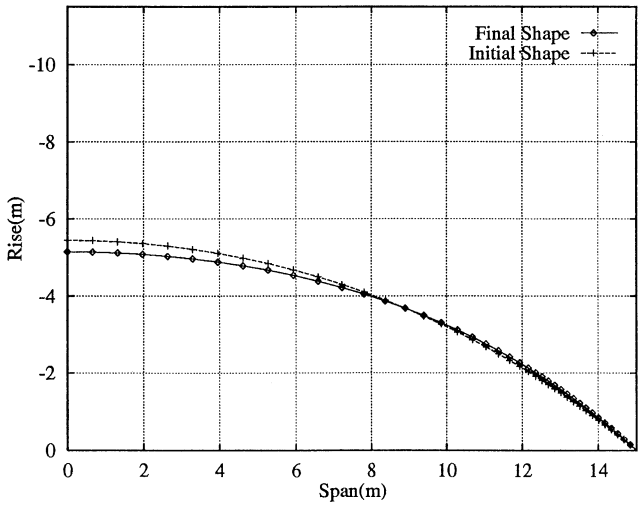

Fig. 11: Sectional Shape along the Longitudinal Line (Wind Load + Dead Load, Fixed Support)

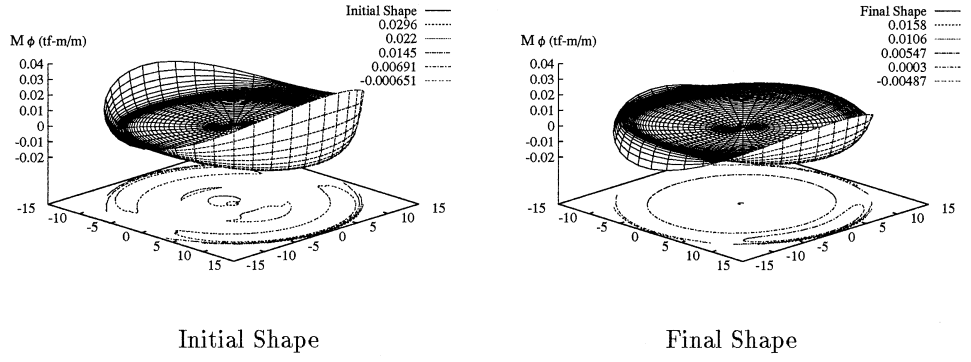

Fig. 12: Bending Moment Distribution in the Longitudinal Direction (Wind Load + Dead Load, Fixed Support)

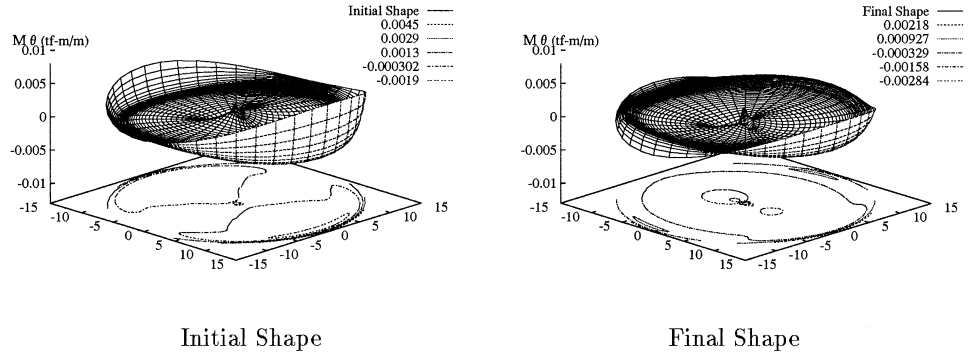

Fig. 13: Bending Moment Distribution in the Meridional Direction (Wind Load + Dead Load, Fixed Support)

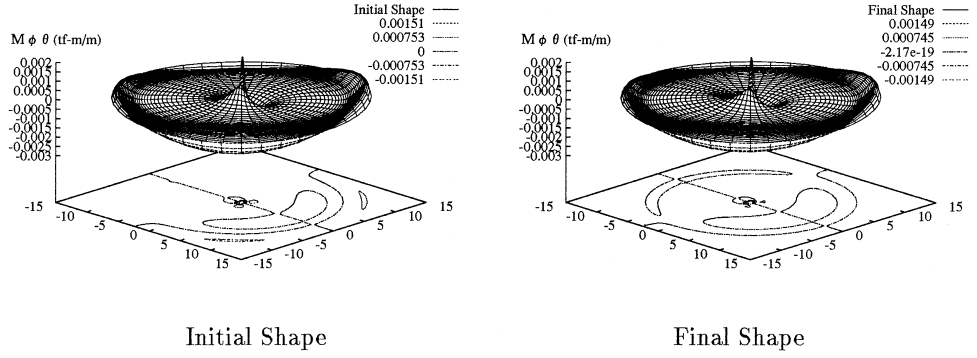

Fig. 14: Twisting Moment Distribution (Wind Load + Dead Load, Fixed Support)

that the bending moment occurred at the initial shape is apparently vanished in the final shape of the shell.

4 Numerical Analysis of Shape Optimization of Spatial Structures

In this section, numerical examples for spatial structures are presented, where both a grid shell having rectangular plan and a lattice shell having circular plan are dealt with under action of self-weight as design loads.

4.1 Grid Shell

Fig. 15 shows the plan of the grid shell which is dealt with as the first numerical example of the shape optimization of space frames, where the initial shape $z = f(x,y)$ of the structure is given by the following equation.

$$z = h(x^2 - a^2)(y^2 - b^2) \tag{11}$$

Numerical analysis is performed for a quarter part of the structure considering the symmetricity of the plan itself, which is subjected to dead load. For the boundary condition of the grid shell, both pinned and fixed conditions are dealt with. Detailed parameters which are used in the numerical analysis are as shown in Table 4 and the total length (221.01 *m*) of the structural elements of the initial structure is used as a constraint condition for the nonlinear programming analysis.

Figs. 16 through 18 show the numerical results of the grid shell which has the fixed boundary, where the shape of the shell, the axial force and the bending moment distributions are depicted, respectively. Figs. 19 through 21 show the same results for the shell supported by pinned end. From Fig. 16 for fixed end and Fig. 19 for pinned one, we can observe that the comparatively large changing in their shapes can be seen especially in the vicinity of the boundaries accompanied with change of curvature of the curved surface of the grid shell. As the results, the bending moment distribution observed around the same region of the shell in the initial stage can be seen to be largely reduced in the final shape. Additionally, it has to be emphasized that geometrical changes between the initial and the final shells can be seen not only in their shape of the curved surface but

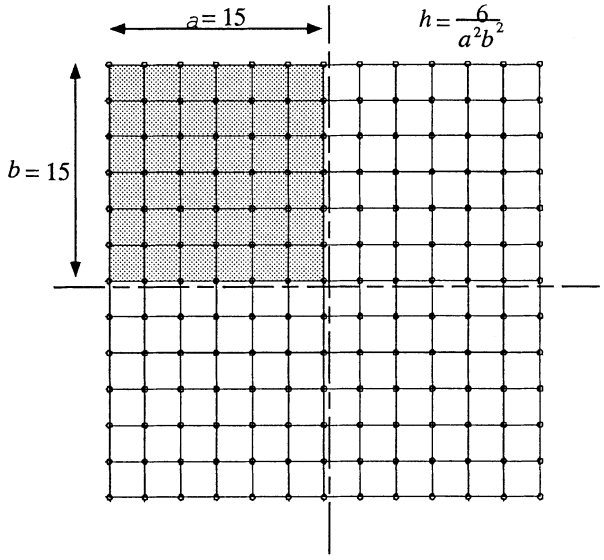

Fig. 15: Plan of Grid Shell

Table 4: Parameters adopted for Grid Shell Analysis

Number of Node	49	Young's Modulus	2.1×10^7 tf/m^2
Number of Element	84	Sectional Area of Beam	0.01 m^2
Degree of Freedome	96 (xyz-free)	Moment of Inertia of Beam	0.00005 m^4
Span	30 m	Poisson's Ratio	0.3
Total of Element Length	221.01 m	Weight Density	7.85 t/m^3

also in their grid arrangements themselves and it can be dominantly observed especially in the case of the shell supported by pin ends compared to that of fixed ends.

4.2 Lattice Dome

As the second numerical example of spatial frames, lattice dome subjected to its self-weight is adopted in this subsection, of which plan is as shown in Fig. 22. Numerical data used in the present analysis is as shown in Table 5. A spherical lattice dome with a diameter of 15 *m* is adopted as the initial shape and numerical analyses are carried out for the half part of the dome as shown in Fig. 22 by gray area. Fixed boundary condition is adopted and the total length of elements in the initial stage, 298.55 *m*, is used as the restraint condition for numerical analysis.

Fig. 23 through 25 show the shape change, the axial force distribution and the bending moment map, respectively, where the initial data is depicted by "a" while the final ones are shown by "b". Fig. 23 shows that the initial shape of the dome changes into the final one with a larger rise compared to that of the original shape and, additionally, the arrangement of the grid itself changes largely as well, where grid pattern used in the initial stage just for convenience in the finite element meshing has changed into the pattern in which several plane arch frames are regularly ar-

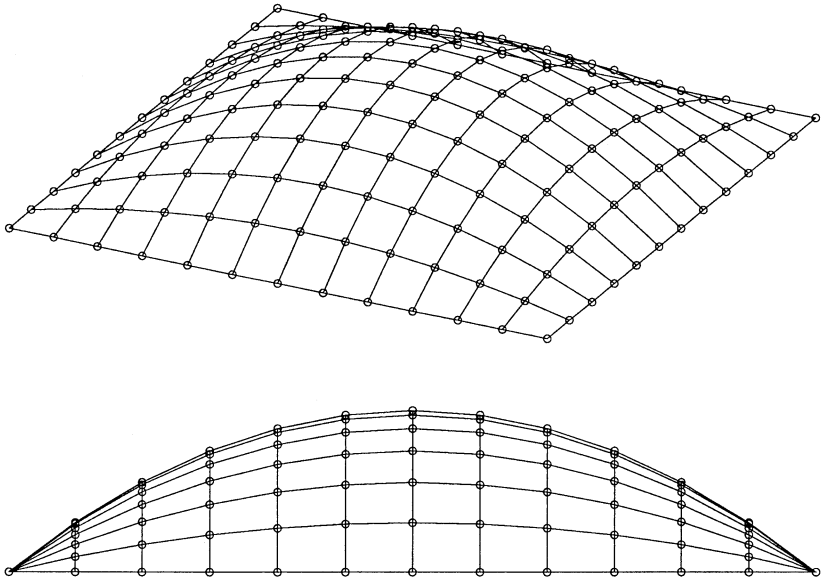

(a) Original Shape

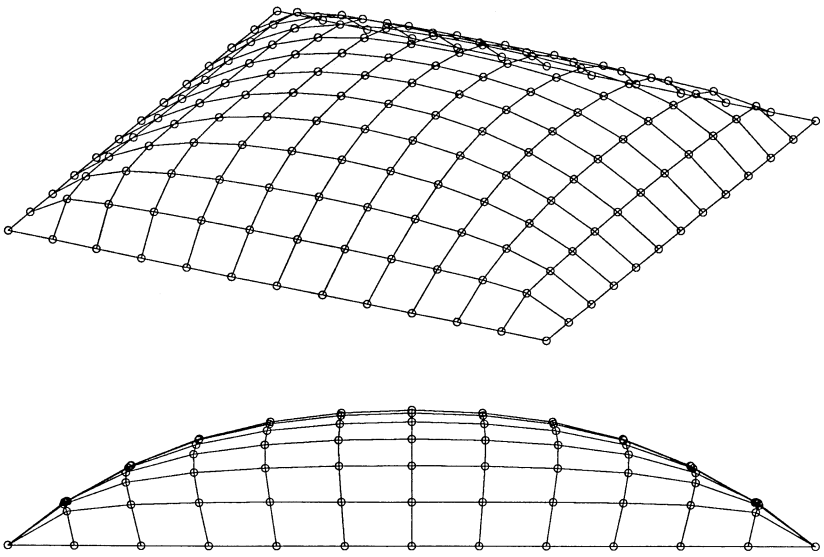

(b) Final Shape

Fig. 16: Shape of Grid Shell (Fixed Support)

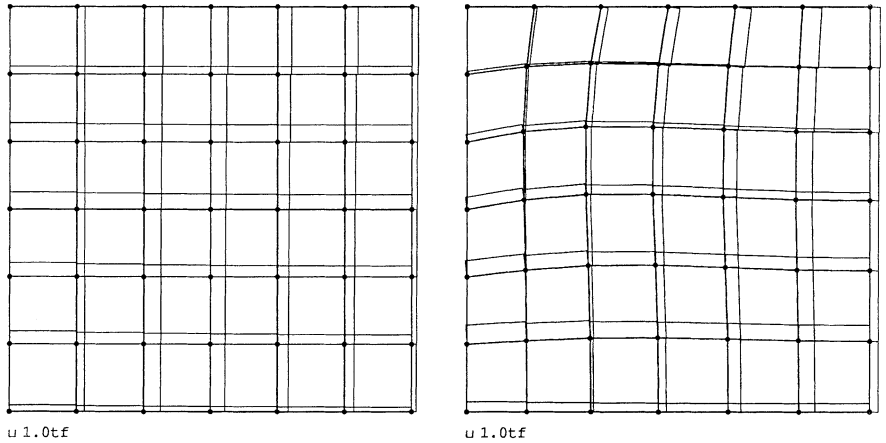

(a) Original Shape (b) Final Shape

Fig. 17: Axial Force (Fixed Support)

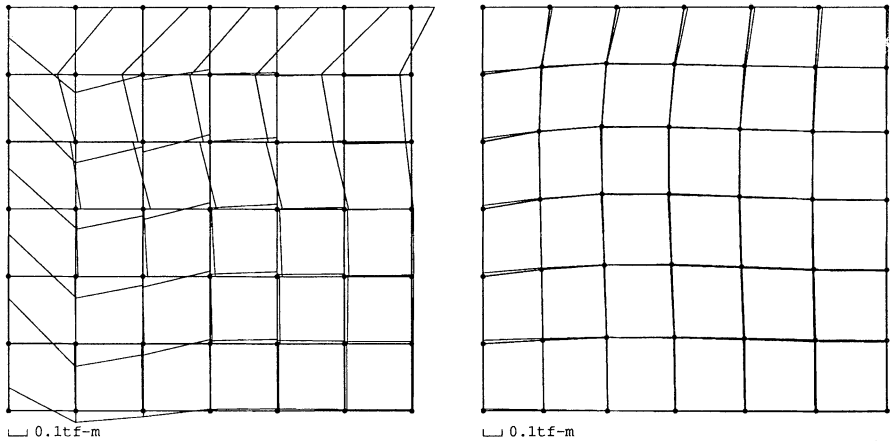

(a) Original Shape (b) Final Shape

Fig. 18: Bending Moment (Fixed Support)

ranged with an arranging angle of 60 degrees in their plan. Consequently, the bending moment distribution which can be observed to occur in almost area is shown to be apparently reduced with the change in the shape of the structure. From the present results, it is shown that the change in the grid arrangement pattern itself can largely affect the bending moment distribution besides the shape of the structure itself as observed in the previous example of the grid shell. This fact for the spatial structure should be emphasized for the characteristics which can not be observed in the shell which is a continuous elastic body.

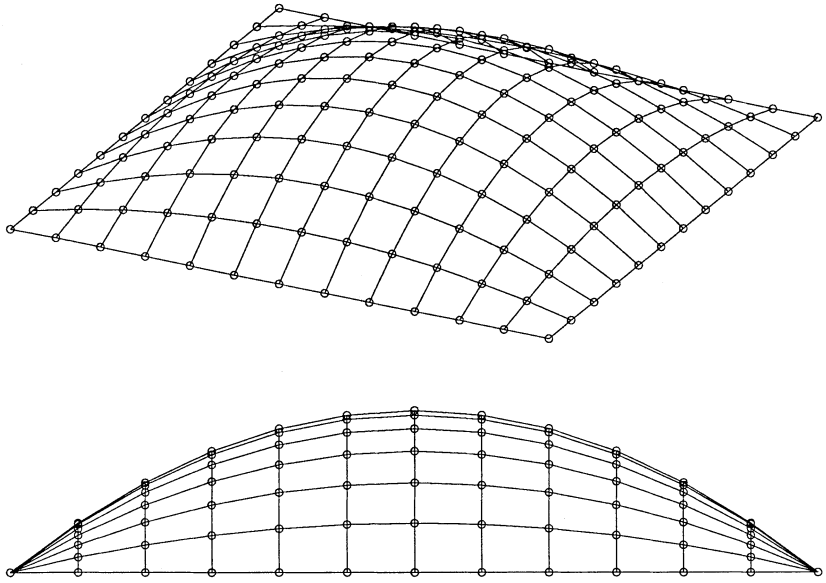

(a) Original Shape

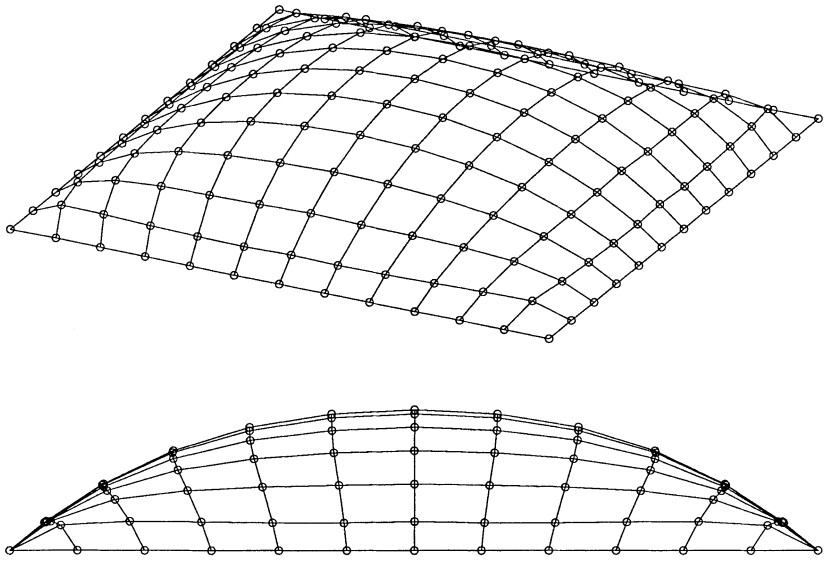

(b) Final Shape

Fig. 19: Shape of Grid Shell (Pinned Support)

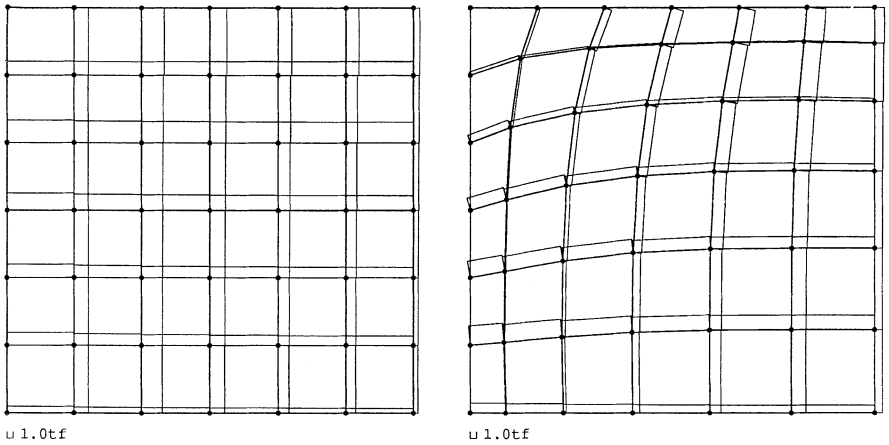

(a) Original Shape (b) Final Shape

Fig. 20: Axial Force (Pinned Support)

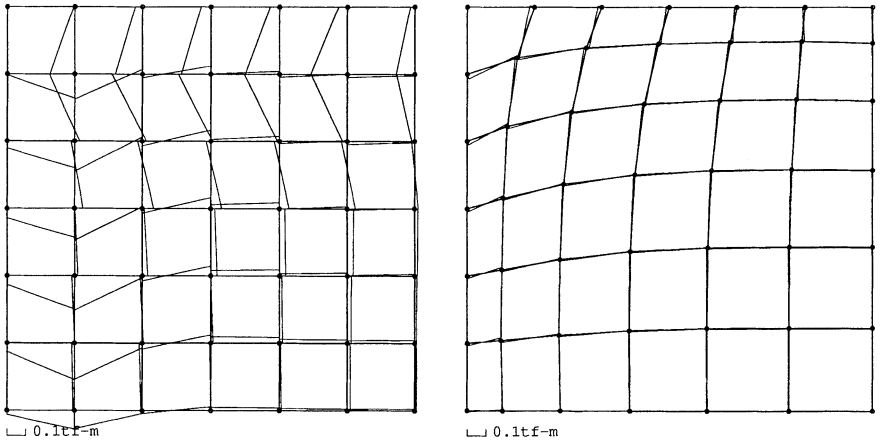

(a) Original Shape (b) Final Shape

Fig. 21: Bending Moment (Pinned Support)

Table 5: Parameters adopted for Lattice Shell Analysis

Number of Node	51	Young's Modulus	2.1×10^7 tf/m^2
Number of Element	125	Sectional Area of Beam	0.01 m^2
Degree of Freedome	96 (xyz-free)	Moment of Inertia of Beam	0.00005 m^4
Span	30 m	Poisson's Ratio	0.3
Total of Element Length	298.55 m	Weight Density	7.85 t/m^3

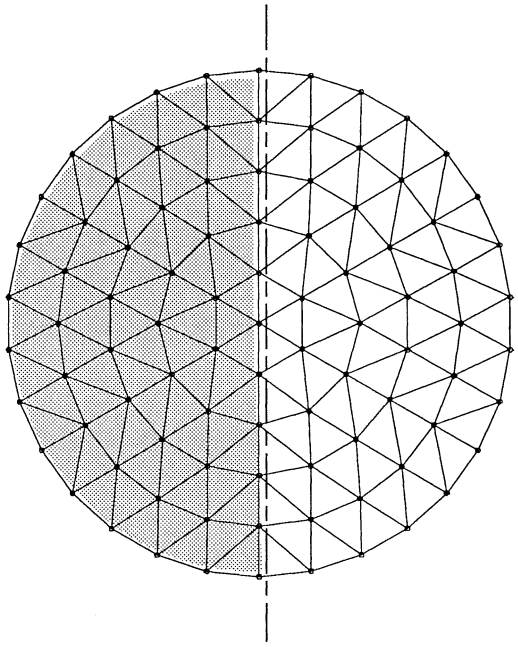

Fig. 22: Plan of Lattice Dome

4.3 Investigations of Numerical Results

The possibilities of reducing the bending moments in large span structures are clearly shown through the numerical analyses by finite element analysis for axisymmetric shell and spatial structures by controlling their shapes themselves, where the least square technique is utilized as the minimization method. From the results derived for the axisymmetric shell which is supported by the inclined roller end, most of bending moment can be observed to be suppressed to appear by controlling the shape of the shell. It can be referred as an origin when we consider the mechanism of occurrence of bending moment in shells or shell-like structures, while the supporting condition is not realistic. Additionally, it is shown that bending moment can be suppressed up to a certain amount even in the other boundary conditions, that is, pinned and fixed boundaries, where it should be pointed out that the bending moment observed around the boundaries in the initial shape can be suppressed up to a certain amount in compensation for the fact that small amount of bending moment can be seen in the part of shell which was “membrane area”, that is, almost no bending moment was observed at their initial situation as if they were scattered over whole surface of the shell. Moreover, it is also important to indicate that suppressing the bending moment can be done even in the case in which the bending moment distribution changes largely because of the discontinuous change of the external load as has been shown in Fig. 9 where snow load is partially subjected on the shell. The same investigation can be shown for the results of the spatial structures as for the shells. However, it should be pointed out especially for the spatial structures that they can reconstruct their resistance form against external design load not only by changing their shapes themselves but also by changing the grid pattern which the spatial structures are composed of. This can be said to be characteristics of spatial structures which are essentially composed of only bar elements and, at the same time, this is the point which shows the difference between continuous

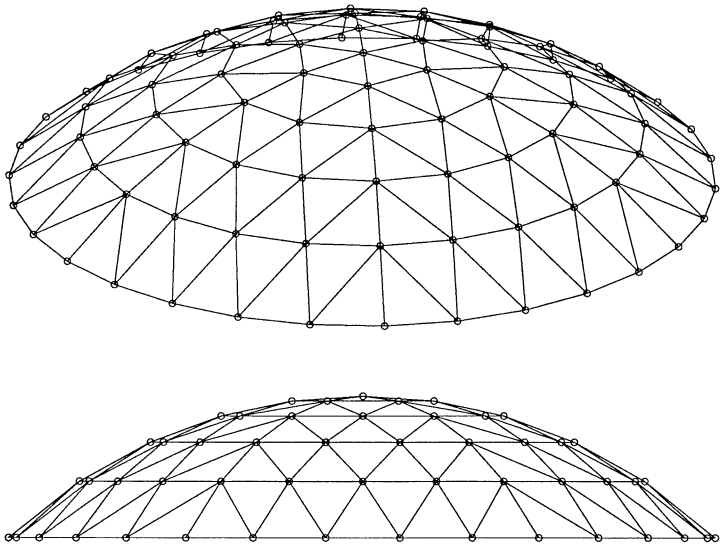

(a) Original Shape

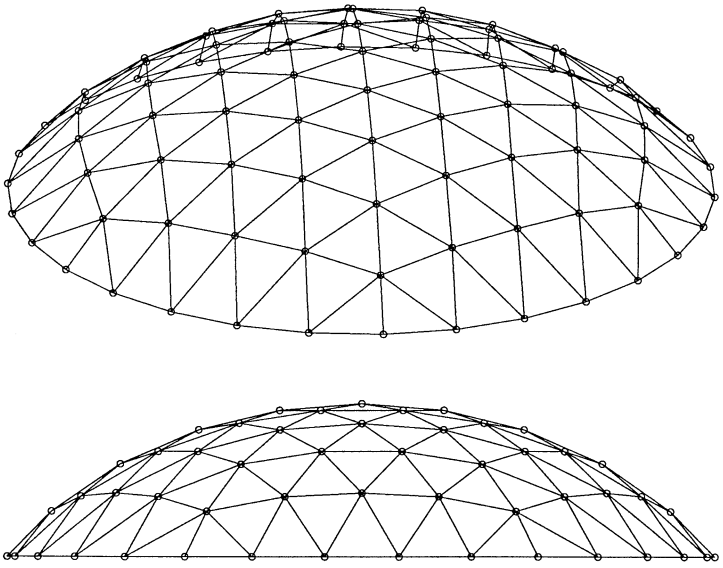

(b) Final Shape

Fig. 23: Shape of Lattice Dome

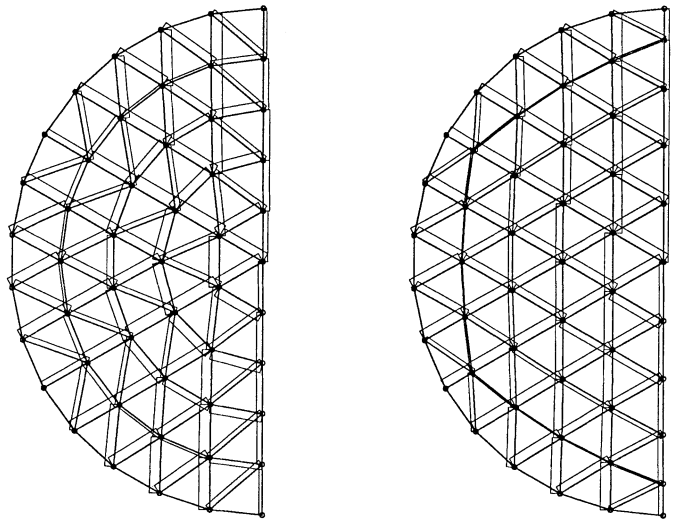

(a) Original Shape (b) Final Shape

Fig. 24: Axial Force of Lattice Dome

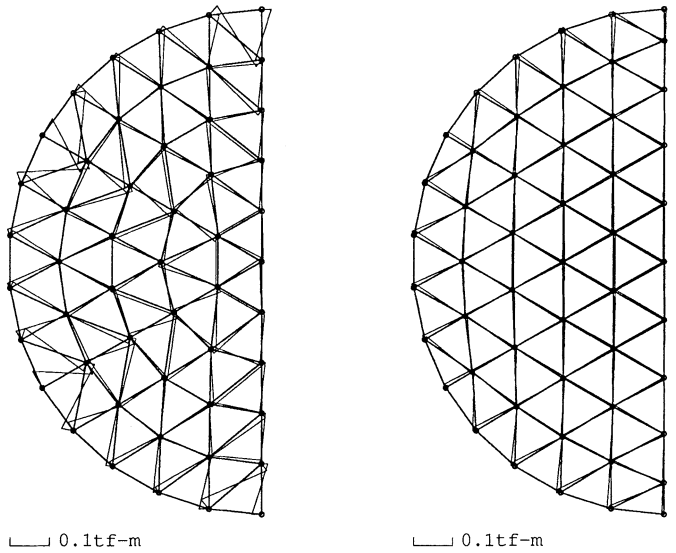

(a) Original Shape (b) Final Shape

Fig. 25: Bending Moment of Lattice Dome

shells and discontinuous spatial structures.

5 Effects of Other Parameters

5.1 Shell Thickness

Through the present numerical analyses, we experienced some difficulties in finding the solution which corresponds to the case in which thickness of shells are extremely small, where the bending moment distribution can be seen especially in the region very near the boundaries and their amount is naturally very small. As the results, the sensitivity of the change of bending moment to the nodal displacement which originates the change of the form of the shell comes to be very small and this is the reason why numerical analysis for this case does not work well. Fig. 26 shows the sensitivity values numerically for the case of the shells of which thickness are 10 *cm* and 5 *cm*, respectively. Fig. 27 shows the comparison between the final shapes of the shells for the thicknesses of 10 *cm* and 30 *cm*, respectively, where no definite difference can be observed. As we can figure out from these results, it can be confirmed that the present shape analysis for the shell with thin shell-thickness can be replaced by that of the shell with larger shell-thickness in the sense of pursuing the moment-free shape. Although the effect of shell-thickness is ignored in the present analysis, it should be taken into account for the more realistic shape analysis.

5.2 Sensitivity with respect to Nodal Coordinates

Sensitivity analysis of bending moment with respect to the nodal coordinate which originates the shape of the axisymmetric shells is carried out to confirm the results obtained in the previous discussions, where relatively large changes in the bending moment distribution are observed in stead of small changes in shape of the shells. Sensitivity of the bending stress resultants can be expressed as follows either for the case where the node of interest belongs to the element of which bending moment is under consideration or for the case where the element does not have the node

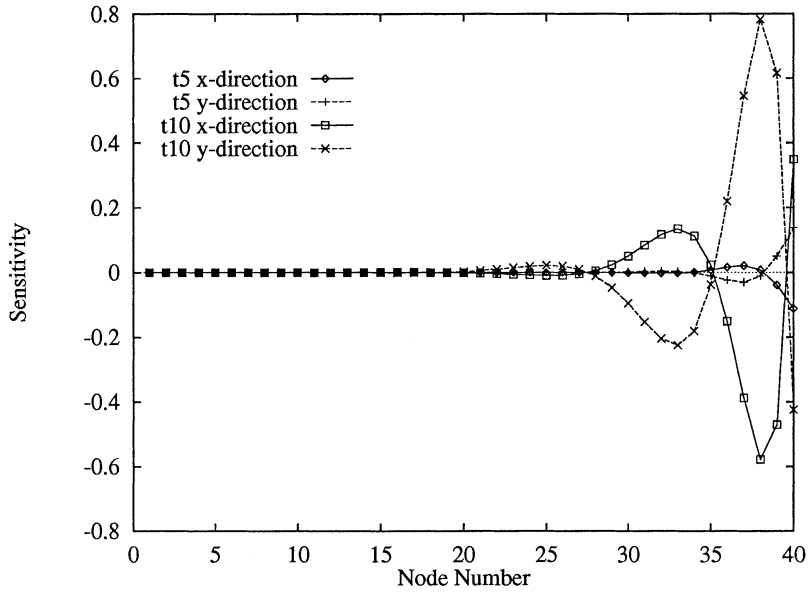

Fig. 26: Comparison of Sensitivity of Different Shell-Thickness

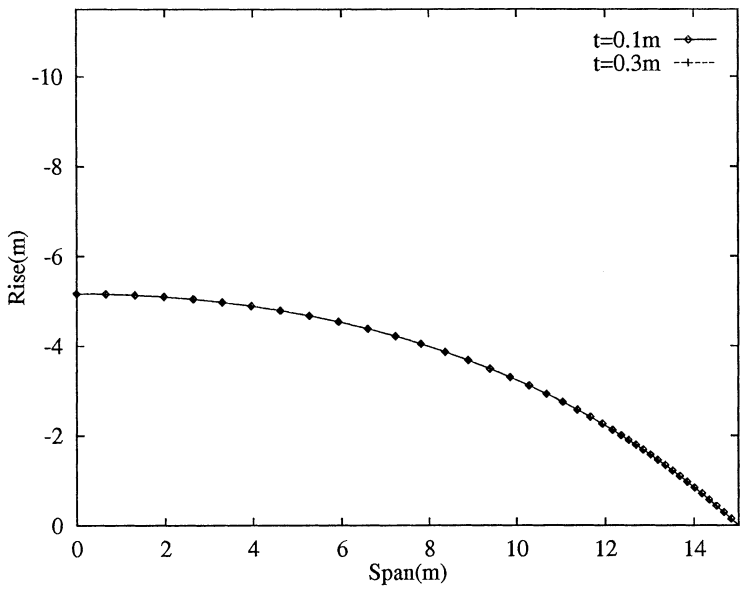

Fig. 27: Effect of Shell-Thickness to Final Shape

as that of itself;

for the case where the node is one of those of the element:

$$\frac{\partial \sigma}{\partial \boldsymbol{r}} = \boldsymbol{D}\left(\frac{\partial \boldsymbol{B}}{\partial \boldsymbol{r}}\,\boldsymbol{d} + \boldsymbol{B}\frac{\partial \boldsymbol{d}}{\partial \boldsymbol{r}}\right) \tag{12}$$

for the case where the node is not one of those of the element:

$$\frac{\partial \sigma}{\partial \boldsymbol{r}} = \boldsymbol{D}\boldsymbol{B}\frac{\partial \boldsymbol{d}}{\partial \boldsymbol{r}} \tag{13}$$

Fig. 29 shows the sensitivity of the bending moment in the longitudinal direction with respect to the nodal displacement in the vertical direction for the spherical shell which was used as the initial shape in section 4. The value of the sensitivity in the figure is that in the middle point of each element, where each node is arranged with an equal distance each other, the nodes are numbered in ascendant order from the central axis of revolution and the sensitivities are shown for the number 1, 10, 20, 30 and 40, respectively. From this figure, we can observe that large sensitivities are seen in the elements adjacent to the node of interest and the sensitivity with a different sign can be observed in the elements next to those. Additionally, almost no sensitivity can be observed in those elements which are far from the node under observation. The value of the sensitivity is about 1.0 $tf \cdot m/m^2$, which means the change in the bending moment will be about 0.001 $tf \cdot m/m$ for 1 mm of displacement of the node in the vertical direction. Fig. 30 shows the result of stress analysis of the spherical shell in which the node of number 10 is actually displaced by 1 mm in the vertical direction. Fig. 31 shows the sensitivity for the shell with the shape obtained as the final one through the shape analysis in the same way as the previous one for the spherical shell, where

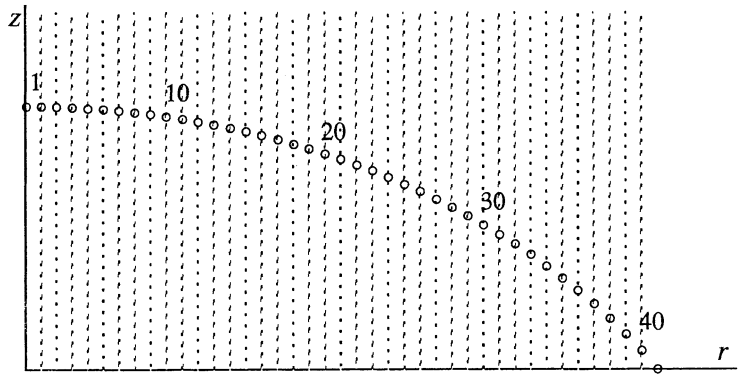

Fig. 28: Model for Sensitivity Analysis

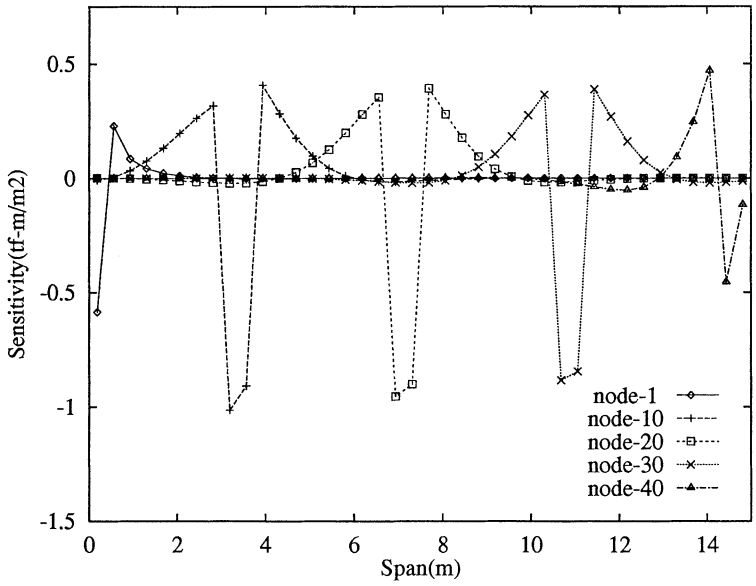

Fig. 29: Sensitivity of M_φ with respect to Specified Nodal Displacement

each figure corresponds to the result for fixed, pinned and inclined roller supporting condition, respectively. As seen in the previous result for the spherical shell, almost the same sensitivity as the spherical shell can be observed for each shell. Consequently, we can conclude from the sensitivity analysis in the present section that the sensitivity of the nodal displacement to the bending moment is relatively large, which is, however, restricted in the adjacent elements to the node, and the curved surface of shells should be made curved correctly and smoothly so that shells act against the external loads in the way expected to them, in another word, as “shape resistant structure”.

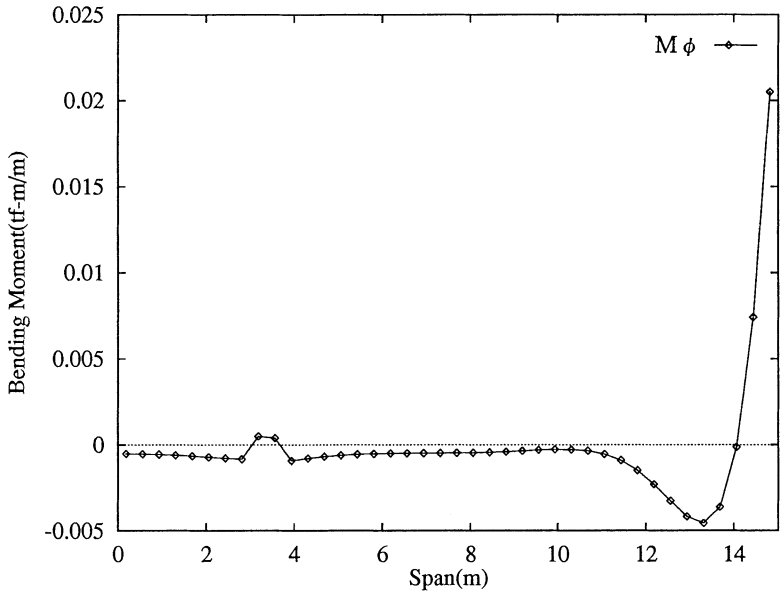

Fig. 30: Effect of Enforced Nodal Displacement on M_{φ}

6 Feasibility Study for Original Surface of Design

Stress analysis of RC shells under dead load are carried out so that we can confirm the efficiency of the shape analysis as has been shown up to here in the actual shell design. The numerical results are shown for the RC shell of which shell-thickness are 5 *cm* with single layer reinforcements and 12 *cm* with double layer ones, respectively. Naturally, shells are highly indeterminate structures and, as the results, the shapes resulted from those with different shell-thickness can be different. The differences between them, however, can be expected to be not so large ones as already shown by the observations in the previous section. The shapes of RC shells adopted in the present section as examples are both the spherical shell and that obtained through the previous shape analysis, both of which are supported by fixed end, and the shells with three different values of surface area are dealt with, that is, model-A of 750 m^2, model-B of 800 m^2 and model-C of 850 m^2, respectively. Additionally, comparison to confirm the effect of the scale is done for the shells with different maximum span, that is, 30 *m*, 60 *m*, 90 *m* and 120 *m*, respectively, while the shell-thickness are fixed as both 5 *cm* and 12 *cm* for all shells investigated in this section. The shapes of the shells adopted here are shown in Fig. 32 in their elevations, where the initial shapes are depicted together with the final shape of the numerical results for each model.

6.1 Fiber Stresses

Tables 6 through 11 show the stress values, where tables are composed of in such a way that the column corresponds to whether the place investigated is near the apex or the boundary with a discrimination of the membrane stress and the bending fiber stress and the row shows whether the shell is the initial spherical one or the final shape one with the different values of the span of four kinds. In the table, for the stresses near the apex, those of the element which is the second one

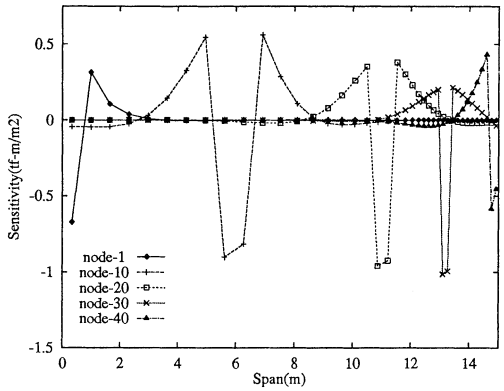

(a) Fixed Supporting

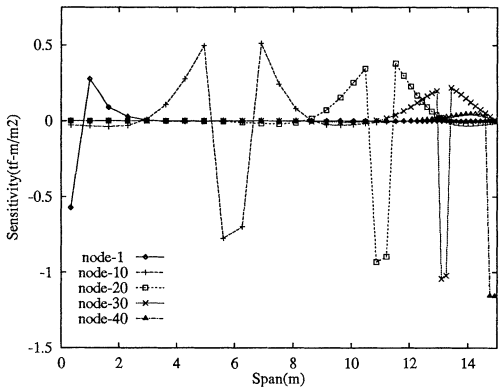

(b) Pinned Supporting

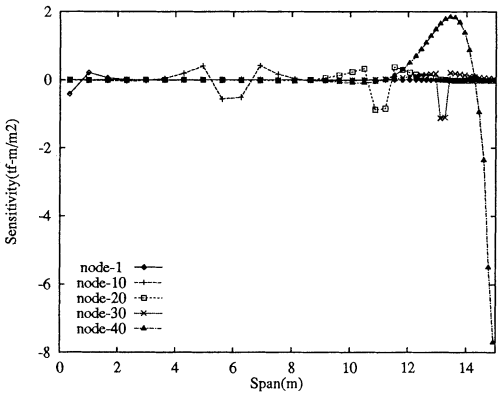

(c) Inclined Roller Supporting

Fig. 31: Sensitivities of M_{φ} in Bending-Free Shells with respect to Specified Nodal Displacement for Each Boundary Conditions

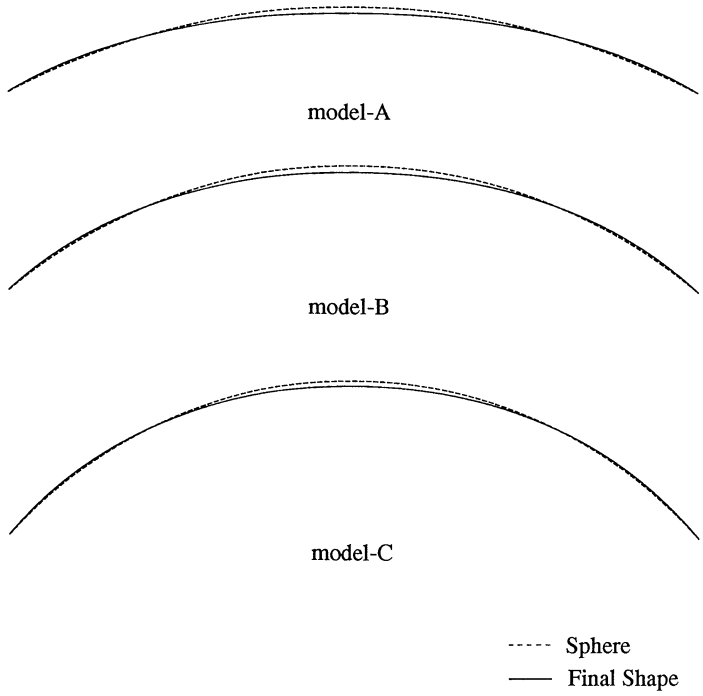

Fig. 32: Elevations of Shells adopted for Feasibility Study

from the central axis of revolution are shown and, for those of near the boundary, the values in the middle point of the element which is adjacent to the boundary are depicted. As the material constants, 2.1×10^6 tf/m^2 for Young's Modulus, 0.17 for Poisson's ratio and 2.4 t/m^3 for density are adopted for the numerical analysis. For the shells with larger rise/span ratio, less bending distribution near the boundary can be observed and, for those with less ratio of rise/span, that is, shallower shells, large distribution of bending moments occur near the boundary while they can be observed to mostly vanish for the corresponding shells with final shapes. Consequently, no tension stress occurs in the shells with the final shapes of the numerical results as long as they are subjected to their own weight loading and tendency of this phenomenon is more likely in the shell with larger thickness. It is, however, natural that all kinds of the other design loads should be considered besides the dead load and then some regards should be taken care of on to the occurrence of tension stress in the actual design stage. Consequently, the shapes shown in the present results for the shell with no tension stress resultants under dead load are those which should be considered as the shells with an original surface of design around which the actual surfaces of the shells are brainstormed.

6.2 Displacements

It is important to check the amount of the displacement of the structures discussed here in order to make sure that the shape analysis for the structures with bending free condition has a certain meaning from the view point of actual design. In Fig. 33, numerical results of displacements of the axisymmetric RC shells subjected to the dead load under fixed end supporting condition are depicted, where those with both the initial shape and the final one are separately shown.

Table 6: Stresses in RC Shell of Model-A (5 *cm* thickness)

Model-A (t = 5 cm)		Vicinity of Apex		Boundary	
	span (m)	Membrane Stress kgf/cm^2	Bending Stress kgf/cm^2	Membrane Stress kgf/cm^2	Bending Stress kgf/cm^2
Sphere	30.0	–3.867	–0.022	–3.978	3.437
	60.0	–7.736	–0.041	–8.036	6.081
	90.0	–11.607	–0.084	–12.103	8.383
	120.0	–15.478	–0.157	–16.175	10.442
Final Shape	30.0	–5.210	–0.145	–3.723	0.268
	60.0	–10.421	–0.216	–7.448	0.337
	90.0	–15.631	–0.332	–11.173	0.430
	120.0	–20.842	–0.490	–14.898	0.541

Table 7: Stresses in RC Shell of Model-B (5 *cm* thickness)

Model-B (t = 5 cm)		Vicinity of Apex		Boundary	
	span (m)	Membrane Stress kgf/cm^2	Bending Stress kgf/cm^2	Membrane Stress kgf/cm^2	Bending Stress kgf/cm^2
Sphere	30.0	–2.808	–0.021	–3.141	1.233
	60.0	–5.618	–0.044	–6.302	1.995
	90.0	–8.429	–0.096	–9.465	2.608
	120.0	–11.239	–0.182	–12.629	3.123
Final Shape	30.0	–3.511	–0.079	–3.012	0.107
	60.0	–7.023	–0.140	–6.024	0.115
	90.0	–10.535	–0.261	–9.036	0.125
	120.0	–14.047	–0.410	–12.049	0.135

Table 8: Stresses in RC Shell of Model-C (5 *cm* thickness)

Model-C (t = 5 cm)		Vicinity of Apex		Boundary	
	span (m)	Membrane Stress kgf/cm^2	Bending Stress kgf/cm^2	Membrane Stress kgf/cm^2	Bending Stress kgf/cm^2
Sphere	30.0	–2.407	–0.022	–2.884	0.185
	60.0	–4.816	–0.047	–5.770	0.143
	90.0	–7.225	–0.103	–8.654	0.090
	120.0	–9.634	–0.193	–11.539	0.038
Final Shape	30.0	–2.804	–0.059	–2.830	0.064
	60.0	–5.607	–0.128	–5.660	0.066
	90.0	–8.412	–0.236	–8.490	0.068
	120.0	–11.217	–0.378	–11.321	0.069

Table 9: Stresses in RC Shell of Model-A (12 *cm* thickness)

Model-A (t = 12 cm)		Vicinity of Apex		Boundary	
	span (m)	Membrane Stress kgf/cm^2	Bending Stress kgf/cm^2	Membrane Stress kgf/cm^2	Bending Stress kgf/cm^2
Sphere	30.0	–3.866	–0.041	–3.898	3.942
	60.0	–7.733	–0.048	–7.930	7.080
	90.0	–11.601	–0.059	–11.979	9.935
	120.0	–15.471	–0.077	–16.036	12.589
Final Shape	30.0	–5.205	–0.300	–3.719	0.583
	60.0	–10.419	–0.330	–7.445	0.625
	90.0	–15.630	–0.380	–11.170	0.678
	120.0	–20.841	–0.449	–14.895	0.745

Table 10: Stresses in RC Shell of Model-B (12 *cm* thickness)

Model-B (t = 12 cm)		Vicinity of Apex		Boundary	
	span (m)	Membrane Stress kgf/cm^2	Bending Stress kgf/cm^2	Membrane Stress kgf/cm^2	Bending Stress kgf/cm^2
Sphere	30.0	–2.807	–0.040	–3.117	1.583
	60.0	–5.615	–0.047	–6.274	2.599
	90.0	–8.425	–0.060	–9.434	3.463
	120.0	–11.235	–0.082	–12.595	4.229
Final Shape	30.0	–3.510	–0.142	–3.011	0.249
	60.0	–7.022	–0.172	–6.024	0.254
	90.0	–10.534	–0.222	–9.036	0.261
	120.0	–14.046	–0.290	–12.048	0.269

Table 11: Stresses in RC Shell of Model-C (12 *cm* thickness)

Model-C (t = 12 cm)		Vicinity of Apex		Boundary	
	span (m)	Membrane Stress kgf/cm^2	Bending Stress kgf/cm^2	Membrane Stress kgf/cm^2	Bending Stress kgf/cm^2
Sphere	30.0	–2.406	–0.040	–2.880	0.425
	60.0	–4.814	–0.047	–5.767	0.450
	90.0	–7.222	–0.061	–8.653	0.426
	120.0	–9.631	–0.085	–11.539	0.383
Final Shape	30.0	–2.803	–0.095	–2.830	0.152
	60.0	–5.607	–0.125	–5.660	0.154
	90.0	–8.411	–0.174	–8.490	0.155
	120.0	–11.215	–0.241	–11.320	0.157

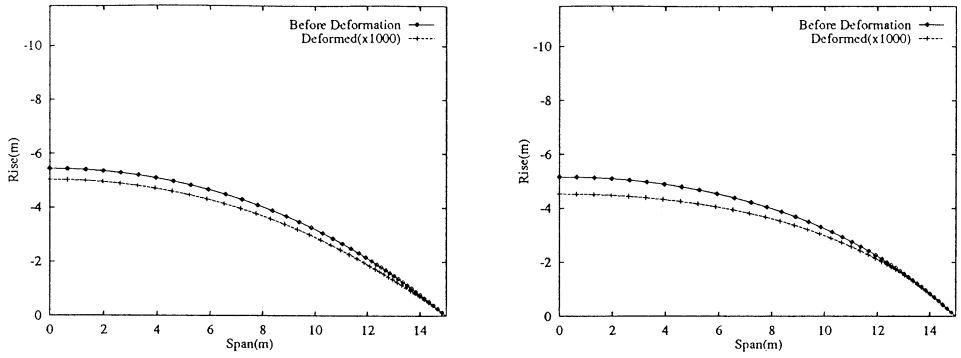

(a) Original Shape (b) Final Shape

Fig. 33: Displacements under Dead Load

The amount of the displacements for both shells can be seen to be very small and, as the consequence, difference in the scale between the initial shape and the final one of the shell is shown much larger than the amount of the displacements of those shells, which imply the final shape is another one as the shape of the shell and can be adopted independently as the shape of the actual shells. Additionally, larger displacements can be observed and smaller changing ratio in the curvature can be seen in the shell with the final shape than that with the initial spherical shell. On the latter matter of the curvature, the shells with the final shape is shown to resist against dead load without large change of the curvature in the vicinity of boundary and it is the reason why those shells with the final shape can resist without bending moment.

7 Conclusion

Theoretical method for pursuing bending-free curved surface which can be used for constructing shells and spatial structures is proposed and numerical results through finite element method are shown to demonstrate the efficiency of the theory, where both axisymmetric shells and spatial structures are adopted as numerical examples. Additionally, some investigations concerned with sensitivity of the change of the nodal displacement for the bending moment distribution and feasibility study toward realization of the bending-free curved surface of RC shells are carried out. Following points can be summarized as a conclusion from the present paper.

1. Shape analysis based upon sensitivity analysis is effective enough to obtain the bending-free curved surface which can be adopted as an original curved surface for shells and spatial structures,

2. bending moments of shells and spatial structures which are originated from definite static external loads as dead load or carrying loads can be effectively suppressed by very small but effective changes of the shape of the structures,

3. even for the partial loading with eccentricity, ability of the minimization technique for the bending moment is still potent, where only small change of the shape of the structures can realize the bending-free curved surface,

4. in the discrete structures like spatial structures which are composed of linear bars, spatial arrangement of the frames largely contributes to the bending moment distribution as well as the shape itself of the structure.

Additionally, we have shown high sensitiveness of the nodal displacement on the bending moment distribution and this numerical result implies that it is very important to accurately construct the shape of shells or spatial structures in order to realize the stress field as is expected in the design stage preceding the actual construction. All of the shapes of shells and spatial structures discussed in this paper are clearly some special ones and, however, the theoretical scheme presented herein can be a general one which has ability to be adopted for the general shape of the structures without any difficulties. Moreover, possibilities for obtaining continuous curved surface by which shells or spatial structures can resist against design loads within specified level of specified stress resultants will be able to shown in the same way presented in this paper. These researches are those which should be done in the future work.

Acknowledgements

The Authors would like to acknowledge valuable discussions with Professor John F. Abel of Cornell University, U. S. A.

References

1) Ramm, E. and Schunk, E. : Heinz Isler Schalen, Stuttgart, Karl Kramer Verlag, 1989.
2) Ramm, E. and Reitinger, R. : Force follows form in shell design, Proceedings of IASS-CSME International Congress on Innovative Large Span Structures, pp.13–17, 1992.
3) Isler, H. : Generating Shell Shapes by Physical Experiments, Bulletin of the International Association for Shell and Spatial Structures (IASS), Vol.34, pp. 53–63, 1993.
4) Ohmori, H. and Nakamasu, Y. : Shape Finding Analysis for Shells and Space Frames by Using Hanging Membrane, Proceedings of International Association of Shell and Spatial Structures (IASS) , Spatial Structures: Heritage, Present and Future, Milano, Italy, pp.865–872, 1995.
5) Ohmori, H. and Hagiwara, N. : Numerical Analysis of Minimum Surface by Finite Element Method, Proceedings of International Association of Shell and Spatial Structures (IASS) Congress in Shell and Spatial Structures, 1989.
6) Ohmori, H. : On the Structural Configuration Mechanics by Using Variational Principles, Proc. International Association of Shell and Spatial Structures (IASS), Vol.1, pp.894–905, 1992.
7) Ohmori, H. and Nakamasu, Y. : Shape Finding Method by using Hanging Membrane, Proceedings of SEIKEN-IASS Symposium, pp.245–252, 1993.
8) Ishihara, K., Yagi, T. and Ohmori, H. : Shape Finding Analysis of Membrane Structure by Using Quasi-Newton Method, Proceedings of International Association of Shell and Spatial Structures (IASS) , Spatial Structures: Heritage, Present and Future, Milano, Italy, pp.767–774, 1995.
9) Ishihara, K. and Ohmori, H. : Shape Finding Analysis for Membrane Structures through Minimal Surface Problem, Proceedings of Japan National Congress for Applied Mechanics, Vol.43, pp.3–9, 1994.

10) Ohmori, H. and Ohki, Y. : Shape Finding Analysis by using Hanging Membrane, Proceedings of National Congress for Applied Mechanics, Vol.43, pp.11–18, 1994.
11) Ishihara, K. and Ohmori, H. : Shape Finding Method by using Minimal Surface, Proceedings of Nonlinear Analysis and Design for Shell and Space Structure, SEIKEN IASS Symposium, pp.261–266, 1993.
12) Ishihara, K. and Ohmori, H. : Minimal Surface Analysis by using Finite Element Method, Proceedings of Japan National Congress for Applied Mechanics, Vol.42, pp.65–73, 1992.
13) Salinas, J. G. O. : Translation Surfaces for the Design and Construction of Wide Span, Proceedings of IASS-CSCE International Congress, pp.631–643, 1992.
14) Ramm, E. : Shape Finding Method of Shells, Bulletin of the International Association for Shell and Space Structures, Vol.33, pp.89–98, 1992.
15) Ramm, E. and Mehlhorn, G. : On shape finding methods and ultimate load analyses of reinforced concrete shells, Engineering Structure, Vol.3, pp.178–198, 1991.
16) Ramm, E., Bletzinger, K. and Kimmich, S. : Strategies in Shape Optimization of Free Form Shells, Springer Verlag, 1991.
17) Ramm, E., Bletzinger, K. and Kimmich, S. : Trimming of Structures by Shape Optimization, Proceedings of 2nd International Conference on Computer Aided Analysis and Design of Concrete Structures, Pineridge Press, 1991.
18) Banichuk, N. V. : Introduction to Optimization of Structures, Springer Verlag, 1991.
19) Hunter, I. S. and Billington, D. P. : Computational Form Finding for Concrete Shell Roofs, Proceedings of ACI Spring Convention, Boston, MA, 1991.
20) Kollegger, J. and Mehlhorn, G. : Analysis of a Free-Formed Reinforced Concrete Model Shell, Proceedings of 2nd International Conference on Computer Aided Analysis and Design of Concrete Structures, Pineridge Press, 1990.
21) Svanberg, K. : The Method of Moving Asymptotes - a New Method for Structural Optimization, International Journal of Numerical Methods in Engineering, Vol.24, pp.359–373, 1987.
22) Fleury, C. : Structural optimization - a new dual method using mixed variables, International Journal of Numerical Methods in Engineering, Vol.23, pp.409–428, 1986.
23) Bennett, J. A. and Botkin, M. E. : The Optimum Shape - Automated Structural Design, Plenum Press, 1986.
24) Hildebrandt, S. and Tromba, A. : Mathematics and Optimal Form, Scientific American Library, 1985.
25) Haber, R. B. and Abel, J. F. : Initial Equilibrium Solution Methods for Cable Reinforced Membranes Part I: Formulations; Part II: Implementation, Computational Methods for Applied Mechanics in Engineering, Vol.30, pp. 63–284, 285–306, 1982.
26) Schmit, L. A. : Structural Synthesis - Its Genesis and Development, AIAA Journal, Vol.19, pp.1249–1263, 1981.